Nonlinear interference between solitons and nonstationary dispersive waves in a passively mode-locked fiber laser

Jin Jer Huang [1,*] Zi Lin Jia,[2] and Xin Lu Zhang [2,†]

[1]*Department of Applied Physics, Tiangong University, Tianjin 300387, China*

[2]*Department of Optoelectronic Information Science and Engineering, Tiangong University, Tianjin 300387, China*

(Received 28 September 2021; accepted 19 April 2022; published 27 May 2022)

We numerically investigated the interaction of a soliton with nonstationary dispersive waves as well as the soliton interaction induced by them, in a fiber ring laser mode locked by a nonlinear polarization rotation technique. In low-loss mode-locked states, a resonant frequency shifting effect and two time-jittering motions of solitons are found during the interaction. An analysis reveals that an indirect phase-matching interference between a pulsed dispersive wave and a soliton upon cross-phase modulation breaks the conservation of soliton momentum, while the subsequent soliton reconstruction leads to a recovery of the conservation. The interference mechanism, together with the conservation of soliton momentum, accounts for some basic behaviors of soliton laser dynamics.

DOI: 10.1103/PhysRevA.105.053526

I. INTRODUCTION

The soliton, as a localized field or matter without diffusion, is a fascinating object or phenomenon in nonlinear science. It is widely found in many branches of physics: hydrodynamics, plasma physics, optics, and condensed-matter physics (Bose-Einstein condensation) [1]. In optics, fiber laser systems offer a platform to generate a rich source of temporal optical solitons, generally as pulsed solutions in integrable systems modeled by the nonlinear Schrödinger equation (NSE), nonintegrable ones by the complex Ginzburg-Landau equation (CGLE), and those modeled by mixed equations of them [2]. Optical solitons were found to broadly exist in various mode-locked fiber structures from a balance between nonlinearity and dispersion together with a long-time stability over lumped gain and loss in silicon based fibers. Organized or disorganized multipulse forms, such as the soliton molecule, soliton bunch, soliton gas, liquid, crystal, and even their complexes, triggered by various mode-locking techniques, are forming a multisoliton family [3–6]. Naturally, the internal soliton interaction, an indication of the essence of multisoliton dynamics, has long been studied in experiment and theory due to its scientific significance and applications in optical communication. A wealth of pulse dynamical behaviors have been found in fiber lasers based on phase-sensitive nonlinearity, dissipative nature, and cavity dynamics [2,7–9]. Especially with the advent of time-resolved spectral technology (the time-stretched dispersive Fourier-transform method [10,11]), many dynamical issues associated with soliton structures have regained attention recently [8,9,12–15]. Thus, an in-depth understanding of soliton microdynamics is required to facilitate sophisticated ultrafast all-optical information processing [6,16–18].

So far, the soliton interaction has been known to include a direct interaction through collision, a short-range interaction with an exponential decaying strength [2], and a long-range interaction mediated through a dispersive wave (DW) [19–21]. The last case was theoretically focused by analyzing the DW formation and structure under lumped amplification [22–28]. Another well-known soliton interaction is the fiber optoacoustic interaction or the electrostrictional effect [24,29–32], which exerts weak forces (10^{-9} order variation of refractive index) among conventional (Kerr) solitons caused by localized transverse acoustic pulses and incurs a soliton bunching when its repetition rate induces acoustic resonance [24,30,32]. Recently, it was found that the continuum noise background modulated by gain depletion induces weak attractive forces between soliton pairs in a form of Brownian motion [33,34] and the global noise-mediated interaction was considered to be complementary to the repulsive force induced by DWs [27,33] to form tight soliton bunches. Among them, the interaction between a soliton and moving DWs or continuous wave (CW) components is more fundamental in terms of its universality in fiber lasers, of concern in this paper. Sometimes, CWs, DWs, linear waves, and nonsoliton waves are not distinguished in the literature. From now on, we restrict the term "CW" to an injected one from an extracavity source or an intracavity background CW; DW means the resonant nonsoliton component of a solitary wave which makes up the sidebands, a special CW. As such, the concept of a soliton in this context will include a copropagating DW that sticks together, the core of which without the DW will be called an eigensoliton, or simply a conventional (Kerr) soliton. A soliton can then be said to be stationary or nonstationary according to its pedestal (or DW) type. Early investigations showed that a weak CW-soliton interaction can perturb the soliton in the parameters of position, phase,

*huangjinzhe@tiangong.edu.cn

†zhangxinlu@tiangong.edu.cn

frequency (group velocity), and amplitude [22,35,36] and that a strong one may obviously advance or delay the soliton by pulsed CWs [37,38] or periodically compress it by a CW background [39]. The global intracavity CW-soliton interaction commonly occurs in a low-loss cavity and contributes to passive harmonic mode locking (HML) or a pulse pattern formation [9,21,40] by the repulsive effect between solitons within a small frequency difference [41]. Actually, an intentional injection of an outside coherent source can be used to control internal soliton trains [42]. Also, in a higher-order dispersion environment (in photonic crystal fibers) around a zero dispersion point, the CW mediated interaction may cause a frequency shifted reflection by cross-phase modulation (XPM) [43,44], Cherenkov or resonant radiation [45,46], and four-wave mixing (FWM) [47,48], which nevertheless is weak for low-power ps solitons in standard commercial fibers. For the same reason of smallness, the Raman-induced self-frequency shift [2] can be neglected. It has been known that the generation of DWs is inevitable in a periodic pulse circulation and that they present as a long standing-wave-like structure, a series of Gordon-Kelly sidebands [22,49,50] in the spectral domain. In spite of a limited fluctuation from lumped gain and loss, the attached DW is in phase with the host and is periodically steady as a quasistationary DW, which can be simply called a stationary DW. An analytic stationary DW model demonstrates an exponentially decaying tail centered at the soliton with a Lorentzian shape spectrum [27]. In another case, the nonstationary DW is a free DW or an overloaded dispersive soliton wing (pedestal, the Gordon-Kelly sidebands in the spectrum) [28], which oscillates intensely and sheds off a part of itself under modulation. Thus, a soliton can affect nearby solitons by overlapping or shedding nonstationary sub-DWs, as a DW mediated soliton interaction (DWMSI) [21], similar to the interaction of fermions by intermediate bosons in the context of particle physics. The DWMSI is vital for the HML by providing repulsive forces together with the CW-soliton interaction [21,24,40], and for the soliton bunching [28,51,52]. In the nonstationary case, an emitted and isolated DW should be described by the CGLE under gain and loss modulation (including the saturation mechanism) to present an exact DW-soliton interaction, which is inaccessible by some analytic perturbation methods for stationary interactions [22–26]. Comparatively, in a transmission system governed by the NSE, the frequency shift will approach zero after an interaction predicted by a simple perturbation theory [20,36] and even by an exact model with a superposition of CW and soliton [37,38]. However, in a dissipative cavity, the frequency shift is no longer zero due to some instant nonperiodic behaviors like gain, loss, and polarization. Referring to some simulations through a lumped cubic CGLE, the frequency shift induced by an injected CW [53] or by an intracavity CW [41] was found to exist, which cannot be predicted by any analytic method. This reminds us to return to the numerical method to obtain a reliable conclusion.

In application, Komarov and coworkers realized the control of attraction and repulsion on a conventional four-soliton bundle by injection of a CW in a numerical experiment. Though a real experiment is complicated with an induced parasite CW component [54,55], the DW-soliton interaction and DWMSI give us a chance to manipulate solitons to form information bit streams or to program an output power flux. Impressively, a recent work from He *et al.* realized a precise manipulation of soliton supramolecular structures in a temporal optomechanical lattice inside a fiber ring laser [17,18], where DWs and injected addressing CWs were utilized to compress or dissociate soliton pairs by unbalancing the attraction from an optoacoustic interaction. This provides a promising platform for optically simulating many-body systems and shows a foreseeable prospect in optical information storage and manipulation. A modulation of cavity loss and an injection of addressing CWs in this scheme will cause varied DW or CW components. It then draws an attraction to the nonstationary DWs and the induced DWMSI due to their role in structure control and stability. In theory, the XPM and FWM are generally successful in explaining some two-wave interactions [2] but do not penetrate deep into some soliton cases. Kuznetsov *et al.* made use of the "nonlinear interference" to roughly describe the perturbation of DWs to a soliton in the fiber communication case [35]. In fact, the sidebands can be understood by interference between soliton and DW with a phase-matching condition [27,50,56]. The interference concept was also used by others [23,53], which, nevertheless, was not strictly defined. Komarov *et al.* found that the resonant interference between an injected CW and soliton wings accounts for the soliton drifting in the phase-locking case [53]. However, it is different in the DW-soliton case. In short, the related nonstationary DW-soliton interacting process requires a full optics interpretation and needs to be elaborated further.

In this paper, we simulate soliton generation in a fiber laser to investigate the frequency perturbation to polarized solitons by DWs in detail, based on a passively mode-locked all-optical fiber ring laser by use of nonlinear polarization rotation (NPR). The dynamics of nonstationary DW-soliton interaction and DWMSI are presented. Starting from the CGLEs with a simplified but real transfer matrix of the NPR, presented in Sec. II, two hypothetical pulse collisions are simulated between an incident DW and a single soliton, followed by a DWMSI of two solitons with self-interaction of solitons, shown in Sec. III, where the (nonlinear) interference mechanism can explain the breakdown of the conservation of soliton momentum and then uncover the frequency shifting effect. The interference is further discussed in Sec. IV and the Appendices and is found to be due to phase-modulated waves from XPM and self-phase modulation (SPM) as expected, which cause perturbations to soliton parameters.

II. NUMERICAL MODEL

The DW-soliton interaction and DWMSI can be simulated in a gain fiber by the known CGLE [2]:

$$\frac{\partial A_1}{\partial z} = \frac{g-\alpha}{2}A_1 - \sigma\frac{\partial A_1}{\partial \tau} + i\gamma\left(|A_1|^2 + \frac{2}{3}|A_2|^2\right)A_1 + \left(\frac{g}{2\Omega_g^2} - i\frac{\beta_2}{2}\right)\frac{\partial^2 A_1}{\partial \tau^2}, \tag{1a}$$

$$\frac{\partial A_2}{\partial z} = \frac{g-\alpha}{2}A_2 + \sigma\frac{\partial A_2}{\partial \tau} + i\gamma\left(|A_2|^2 + \frac{2}{3}|A_1|^2\right)A_2 + \left(\frac{g}{2\Omega_g^2} - i\frac{\beta_2}{2}\right)\frac{\partial^2 A_2}{\partial \tau^2} \tag{1b}$$

where $A_{1,2}$ indicate the envelopes of the pulse components along the slow and the fast axis in fiber, the variable τ represents the relative time, and z denotes the propagating distance. In Eqs. (1), the parameters α, 2σ, β_2, γ, g, and Ω_g are, respectively, the absorption coefficient of fiber, inverse group velocity difference between the two polarization modes, group velocity dispersion, cubic refractive nonlinearity, gain coefficient, and gain bandwidth. In a standard single-mode fiber (SMF), Eqs. (1) degenerate into NSEs with $g = 0$. In addition, some terms connected with higher-order dispersion and FWM are neglected owing to little impact.

An NPR device is commonly composed of one polarization-dependent isolator (PD-ISO) sandwiched by two polarization controllers (PCs), which is a popular mode-locking technique harnessing the nonlinear phase shift [57–59]. Each PC can be simplified as a combination of $\lambda/4 + \lambda/2$ plates. So, the first PC (PC1) is associated with two rotating angles ϕ_1, ϕ_2, while the second one (PC2) with ϕ_3, ϕ_4 and the PD-ISO with ϕ_0, where all angles are taken with respect to the slow axis of the fiber. According to the Jones matrix method, the NPR can be expressed as a transfer matrix that decides on a total transmittance depending on these angles of PCs. So we have the formulations

$$\boldsymbol{P}_1 = \boldsymbol{R}(\phi_2)\boldsymbol{H}(\pi/2)\boldsymbol{R}(-\phi_2)\boldsymbol{R}(\phi_1)\boldsymbol{H}(\pi/4)\boldsymbol{R}(-\phi_1), \quad (2a)$$

$$\boldsymbol{P}_2 = \boldsymbol{R}(\phi_4)\boldsymbol{H}(\pi/2)\boldsymbol{R}(-\phi_4)\boldsymbol{R}(\phi_3)\boldsymbol{H}(\pi/4)\boldsymbol{R}(-\phi_3), \quad (2b)$$

$$\boldsymbol{P}_3 = \sqrt{\frac{T_0}{2}}\boldsymbol{R}(\phi_0)\begin{bmatrix}1 & -1\\ 1 & 1\end{bmatrix}\begin{bmatrix}1 & 0\\ 0 & 0\end{bmatrix}\boldsymbol{R}(-\phi_0) \quad (2c)$$

with the definitions

$$\boldsymbol{R}(x) = \begin{bmatrix}\cos x & -\sin x\\ \sin x & \cos x\end{bmatrix}, \quad \boldsymbol{H}(x) = \begin{bmatrix}e^{-ix} & 0\\ 0 & e^{ix}\end{bmatrix}, \quad (3)$$

where $\boldsymbol{P}_{1,2}$ represent the transfer matrices of PC1 and PC2, respectively, and $\boldsymbol{P}_3$ is a transfer matrix of the PD-ISO with the maximum transmittance T_0. The transfer matrix is then $\boldsymbol{J} = \boldsymbol{P}_1\boldsymbol{P}_3\boldsymbol{P}_2$ containing a phase transmission $\boldsymbol{H}(\varphi)$, where $\varphi = \varphi_1 + \varphi_2$, and $\varphi_{1,2}$ denote half of the linear phase shift and the nonlinear one induced by birefringence and nonlinearity, respectively. A nonzero eigenvector of the total Jones matrix $\boldsymbol{J}_{\rm tol} = \boldsymbol{J}\boldsymbol{H}(\varphi)$ indicates a stable polarization state. However, it generally yields a complicated expression due to a pulse dependence on φ_2. A further restriction by $\phi_1 = 2\phi_2$, $\phi_3 = \pi/4$ is adopted to optimize the transfer matrix. A squared modular of the nonzero eigenvalue of the total matrix $\boldsymbol{J}_{\rm tol}$ gives rise to a transmittance of the NPR, i.e.,

$$T_{\rm N} = \tfrac{1}{2}T_0\{1 - \cos(2\phi)\sin[2(\varphi + \theta)]\}. \quad (4)$$

In this way, the transfer matrix reduces to

$$\boldsymbol{J} = \frac{1}{2}\sqrt{\frac{T_0}{2}}\begin{bmatrix}e^{-i\theta}(ie^{i\phi} - e^{-i\phi}) & e^{i\theta}(ie^{i\phi} + e^{-i\phi})\\ e^{-i\theta}(ie^{i\phi} + e^{-i\phi}) & e^{i\theta}(ie^{i\phi} - e^{-i\phi})\end{bmatrix} \quad (5)$$

where $\phi = 2\phi_2 - \phi_0$, $\theta = 2\phi_4 - \phi_0$ are two composite angles standing for the modulation depth and the feedback position of the NPR or initial phase, respectively. Above formulations also make the polarization eigenstate dependent only to ϕ. Thus, the single parameter θ in simulation can be used to analyze the mode-locking mechanism without an influence from the polarization variation. It is enough for this configuration to perform a simulation suitable for some practical cases. If not, ϕ_1 and ϕ_3 can be redefined according to a given experimental condition. In each round trip, the NPR will transform the field periodically as

$$\mathbf{A}(z = 0) = \boldsymbol{J}\mathbf{A}(z = L), \quad (6)$$

where L is the cavity length and $\mathbf{A} = (A_1, A_2)^{\rm T}$. The NPR is set at $z = L$ and the gain begins at $z = 0$.

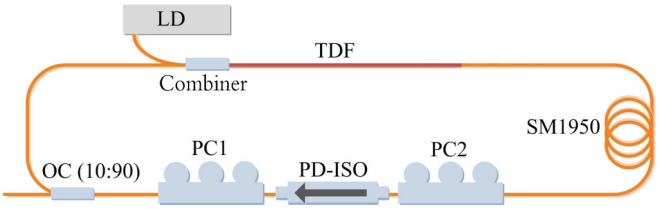

FIG. 1. Schematic of an all-fiber ring laser mode locked by the NPR technique with a TDF (running at 2 μm), pumped by a laser diode at 793 nm.

A passively mode-locked fiber ring cavity is sketched in Fig. 1, composed of a Tm-doped fiber (TDF) pumped by a laser diode through a combiner, a long SMF, an NPR system, and a 10% output coupler (OC). In the following computation, the related parameters are set as $\alpha = 0.01$(dB), $g \leqslant g_0 = 2.0\,{\rm m}^{-1}$, $\Omega_g = 30$ nm, $T_0 = 0.9$ at the center wavelength (2 μm), $\beta_2 = -8.0 \times 10^{-2}$ ps^2 m^{-1} for both the SMF (100 m) and the TDF (8 m) with a mutual beat length $L_{\rm B} = 10$ m, $\gamma = 3.0 \times 10^{-3}$ (W s)$^{-1}$ for the SMF, and 4.5×10^{-3} (W s)$^{-1}$ for the TDF. Furthermore, the inverse group velocity difference is neglected to reduce the soliton drifting. We further relax the gain depletion within the pulse duration and make it an average value, which precludes the gain-induced group velocity variation. The neglected gain depletion causes a weak interaction and renders some interesting dynamical processes but in a longer range (ns level), beyond that of DWMSI [60], so does not affect the issue that we are concerned with here. The gain in TDF then is evaluated as

$$g(z) = g_0\left[1 + \frac{1}{E_{\rm sat}}\int_{-\infty}^{\infty}\left(|A_1|^2 + |A_2|^2\right)d\tau'\right]^{-1}, \quad (7)$$

where $E_{\rm sat}$ is the saturation energy. For a better illustration, a small Gaussian pulse is initially set at 250 ps in the time window to set off a solitary pulse at a given time. Two typical NPR states upon transmittance are considered here to deliver a strong mode locking at $\theta = 0.7\pi$ and a weak one at $\theta = 0.6\pi$, respectively. Their transmittance rates versus the nonlinear phase shift φ_2 are drawn in Fig. 2(a), where the vertical lines roughly denote two working points in the reverse saturable absorption regime at which a soliton can consistently exist. The generation of a soliton is numerically validated and illustrated in Fig. 2(b) by a match of its pulse profile with a typical sech^2 shape, for $\theta = 0.7\pi$ and $E_{\rm sat} = 2.0$ pJ, where the stationary DW is at a lower order of magnitude. In fact, over a certain pumping threshold, single solitons quickly form in both the mode-locking states, as presented in Figs. 2(c) and 2(d), respectively. The demonstrated solitons, just before a passage over the OC, have a duration of 2.29 ps ($\simeq 1.76\tau_0$) for the full width at half maximum (FWHM) and present many

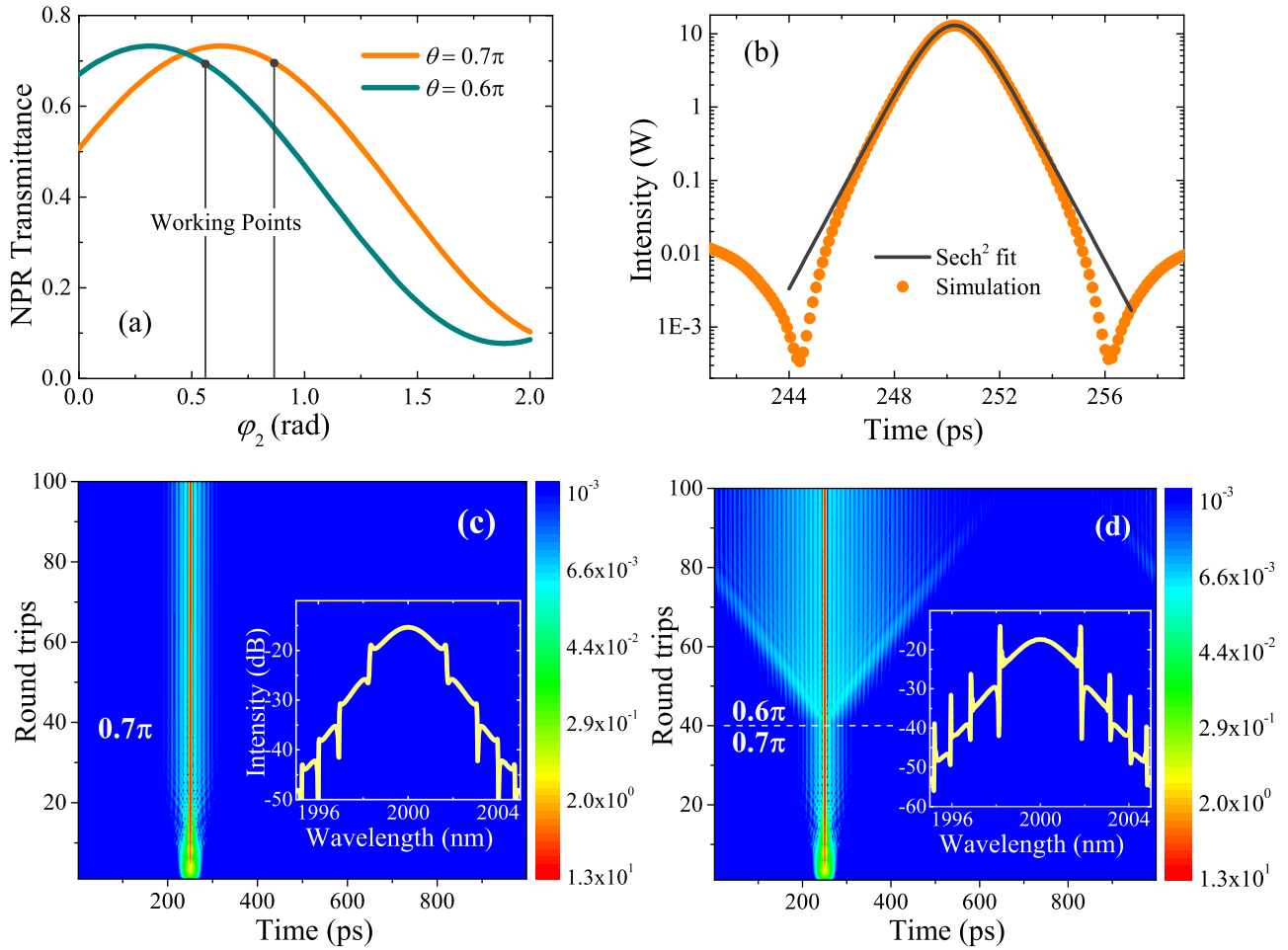

FIG. 2. (a) Two transmittance rates of NPR at $\theta = 0.7\pi$ and 0.6π for the strong and the weak mode locking, respectively, (b) with a simulated soliton profile by a fitting of sech^2, followed by (c) soliton evolution for the strong mode locking and (d) that for the weak one switched from the former, where the insets are the corresponding spectra.

characteristic Gordon-Kelly sidebands, which slightly depend on the angle θ. To display details of the DWs, the intensity distribution is illustrated at the logarithmic scale, which will be adopted in the followed figures. Figure 2(c) shows that the DW lives as two steady wings spread symmetrically around the soliton, which can be called stationary DWs, but it still quickly grows inside the TDF and slowly sheds from the soliton along the SMF, due to the lumped gain and loss. Next, upon a steady pulse circulating, the angle is tuned to $\theta = 0.6\pi$ at the 40th round trip to transfer to the weakly mode-locking state [see Fig. 2(d)]. It is found that the switch to the weakly mode-locking state can disturb the soliton to emit a pair of subpulses symmetrically in two directions and to activate a temporary nonstationary DW. Subsequently, some small DWs consecutively shed from the soliton as well before a new stationary DW forms. The enhanced Gordon-Kelly sidebands in the inset of Fig. 2(d) mean an overloaded pedestal, the reservoir of free DWs [28]. It should be noted that the emitted DW components share the same frequencies (mostly) with the first sidebands, which connect their group velocities by

$$\Omega = 2\pi\nu = -\delta v_g/(\beta_2 v_g^2), \tag{8}$$

where δv_g is a shift of the group velocity v_g, and Ω with the frequency ν is the relative circular frequency with respect to that of the initial soliton. Equation (8) can also be used to determine the frequency shift of a soliton by calculating δv_g. Other frequency components in DWs involving higher-order sidebands are too weak, so are not mentioned here. All the mode-locking states used for the simulations below are between $\theta = 0.7\pi$ and 0.6π.

III. SIMULATIONS AND RESULTS

A. DW-soliton collision: Frequency shift

Now, it is known to us that a soliton with enough energy can shed DWs, which encounter and interact with other solitons since they have different velocities, according to Eq. (8). To thoroughly examine this kind of DW-soliton interaction, two hypothetical collisions of an incident DW and a soliton are simulated and presented in Fig. 3, where Figs. 3(a) and 3(b) exhibit the collision processes attached with sampled spectra in the redshifting and the blueshifting cases, respectively, and the curves in Figs. 3(c) and 3(d) characterize the frequency shifting effect. The incident DW here, simplified as a free Gaussian pulse, is 60 ps long with a central wavelength of ≈2001.82 nm, corresponding to the first red Gordon-Kelly sideband, and is initially laid 125 ps ahead from the soliton. The duration of the Gaussian pulse is taken to be similar to

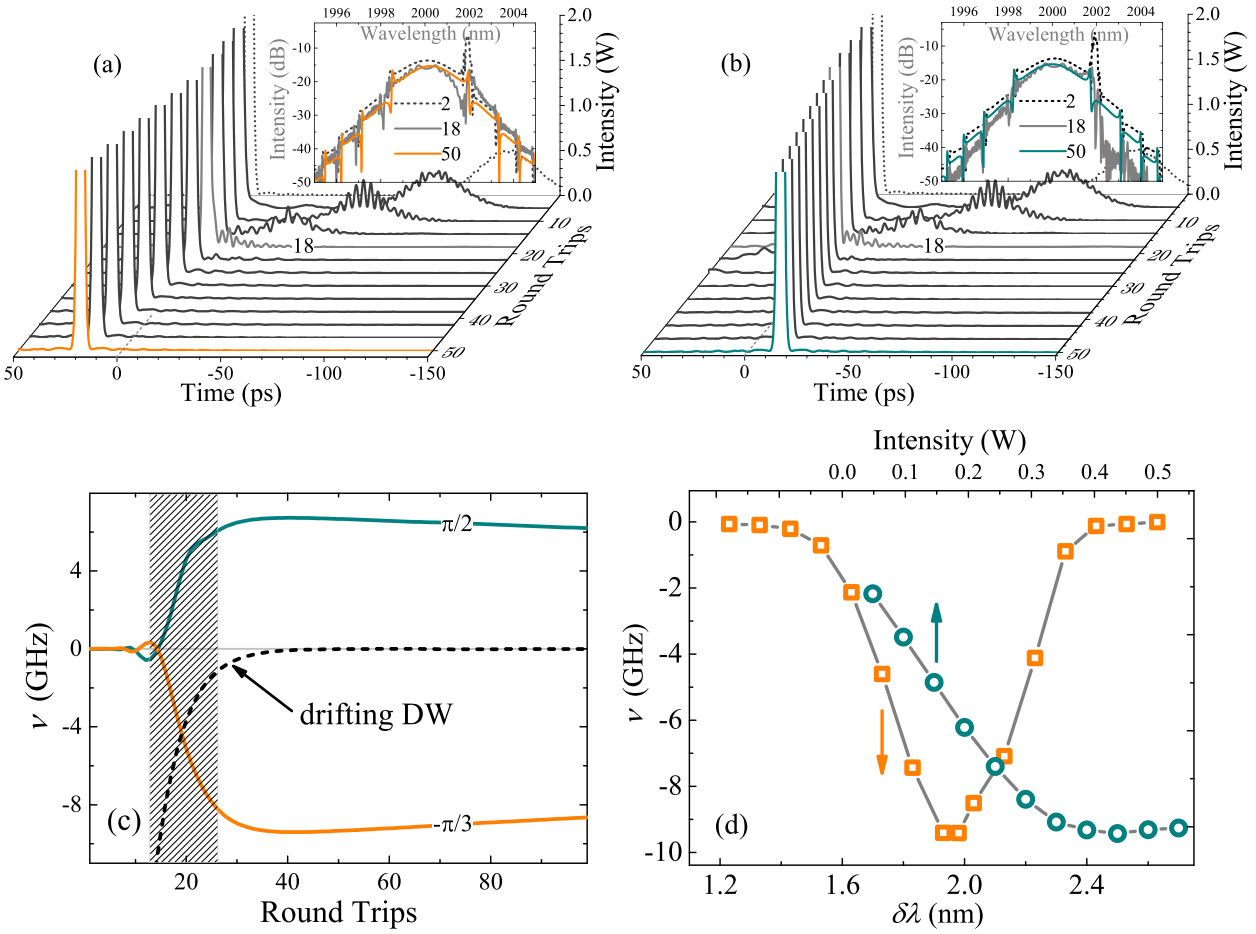

FIG. 3. DW-soliton interaction processes in (a) a redshifting and (b) a blueshifting case with corresponding spectra at the round trips of 2, 18, and 50, appended by related frequency shifts in (c) collisions [panels (a) and (b)] and in (d) a wavelength and an intensity tuning process for the redshifting case.

that of the emitted DWs in Fig. 2(d) and its intensity (0.5 W) is chosen to be much greater than that of the pedestal but far less than the peak power of the soliton when colliding. It simulates a strong DW generation from a change of cavity environment, like an angle switch in NPR. The single soliton has the same parameters as before and the cavity is injected with the DW at the time when the soliton is circulating steadily. Simultaneously, the angle θ is switched to 0.65π from 0.7π for the soliton to collect energy and develop its wings. As expected, the phase difference decides on the frequency shift, so two optimal initial phases $-\pi/3$ and $\pi/2$ are assigned to the DWs in Figs. 3(a) and 3(b), respectively, for a maximum impact on the soliton. It is found that the interaction causes a larger ($\nu \approx -9.4$ GHz) redshift and a smaller ($\nu \approx 6.5$ GHz) blueshift on the soliton, inferring an attractive interaction and a repulsive one, respectively. The momentum or the mean (circular) frequency of a pulse can be estimated by

$$\Omega = \frac{1}{2iE}\sum_{k=1,2}\int_{-\infty}^{\infty}\left(A_k\frac{\partial A_k^*}{\partial\tau} - A_k^*\frac{\partial A_k}{\partial\tau}\right)d\tau$$
$$= \frac{-1}{E}\sum_{k=1,2}\int_{-\infty}^{\infty}\mathrm{Im}\left[A_k^*\frac{\partial A_k}{\partial\tau}\right]d\tau, \qquad (9)$$

where E is the soliton energy, almost a constant. Evidently, the momentum of the soliton is conserved before injecting the DW. The collision dynamics of the interaction can be decomposed into two scenarios, i.e., an interferencelike process between the soliton and the DW, or simply interference that is used below, and a process of reconstructing itself upon approximate conservation of momentum. Since the variation of the soliton is small and the leaving DW is quite weak after the collision, we can assume an approximate conservation of soliton momentum after collision. Theoretically, the nonintegrable CGLE does not strictly but approximately obey the conservation of momentum. The lumped CGLE can be well replaced by a distributed one in a gain saturation case [61,62]. Then, an initial solitary wave that abides by the distributed CGLE has asymptotic conservation of momentum in fiber, analyzed by a method of moments [63]. So, Eq. (9) can be considered approximately invariant for solitary pulses scaled by the round trip period, as can be expressed by

$$\frac{\partial\,\Omega}{\partial N} \simeq 0 \qquad (10)$$

over the round trip number N at least after a collision. The frequency shifts in Fig. 3(c) are evaluated from Eq. (9), which can also be computed by Eq. (8) through the apparent group velocity changes, extracted from the soliton loci in Figs. 3(a)

and 3(b). The shadow in Fig. 3(c) denotes the collision region spanning nearly ten round trips and the curve "drifting DW" is a noncollisional case obtained by laying the DW behind the soliton. Owing to an unsaturated loss of NPR, the depletion of a drifting DW will bring a rapid frequency reduction, which, as a reference value, is used to subtract the varied frequency component of the injected DW for the acquisition of the frequency shift of the interacting soliton, as is done in Fig. 3(c). That is why the two frequency shifts in Fig. 3(c) remain nearly constant after the collision, where the slight decrease can be attributed to a subtraction error and the gain dispersion which will weaken the frequency shifting effect.

Looking back at the figures, it can be found at the height of the collision (round trip 18) that the long-wavelength side of the spectrum is enhanced by the constructive interference in Fig. 3(a) and is depressed by the destructive one in Fig. 3(b), in the first scenario. Thus, a deformed soliton reshapes itself to a redshifted ($\Omega < 0$) or a blueshifted ($\Omega > 0$) one during its recovering process due to the conservation of momentum, as a second scenario. An incident DW with a frequency corresponding to the blue sideband results in similar interference effects (omitted here). Since the intensity of the stationary DW is ten times less than that of the incident one, the internal interference between the two DWs is hardly worthy of consideration, unlike the interference to the eigensoliton. A separating method can be utilized to approximately extract the eigensoliton by a sech^2 fitting if it is needed [64]. Furthermore, if an eigensoliton is deformed during an interaction, the concept of the emergent eigensoliton or emergent soliton proposed by Gordon can be introduced for qualitative analyses [22]. The eigensoliton will be applied below for further discussions, even though it is not well defined here.

To further seek out the cavity dependence of frequency shift, we repeat the DW-soliton collision process in the redshifting case at different wavelengths according to Fig. 3(a). First, the wavelength of the incident DW is sampled from 2001.23 to 2002.63 nm with an interval of 0.1 nm to cover the first sideband, and then the initial phase difference for each wavelength is optimized via a series of numerical collision experiments. The calculated frequency variations are depicted as squared points in Fig. 3(d). In this wavelength tuning case, there is a clear dip pointing to the first sideband with a bandwidth of 0.4 nm, inferring a strong interference selectivity. Second, it is found that the frequency shift increases linearly with the peak intensity of the incident DW below 0.4 W and saturates above, arriving at a maximum interference, drawn in Fig. 3(d) as circle points. The blueshifting case possesses a similar resonant process and a saturation property, but with comparatively small frequency shifts as that in Fig. 3(c). The saturation property of a blueshifting case can be understood by the exhaustion of the soliton spectrum at the first red sideband due to the destructive interference. However, the saturation of the redshifting case in Fig. 3(d) becomes complicated since the soliton, to achieve a certain shift, requires more extended spectra at other wavelengths, which is possible beyond what the enhanced sideband and the background in the cavity can provide in the limited overlapping time. In addition, the same numerical experiment has been carried out as well in an empty fiber cavity, into which a soliton and a 125-ps delayed DW at the red sideband are injected. Without any gain and loss, there is no resonance as expected, and the maximum (absolute) frequency shift is found not greater than 4 GHz with a large enough peak intensity (0.5 W) of the injected DW. The comparison infers a phase-dependent resonant interference and enhancement at the sidebands, like that in the CW-soliton case [53]. Soliton reconstruction, in fact, occurs in the whole course of the interaction within the overlapping time, so is not an independent scenario.

B. Soliton reconstruction: Momentum conservation

For the second scenario, the process of momentum conversation, it is necessary to show that it originates in the essential property of solitons, not in the DWs. To separate the second scenario from the first one (interference), it is better to artificially freeze or delay the recovery processes of the soliton when an interference goes on, which can be realized by performing a kind of spectral tailoring to solitons. In this way, a spectral shaping function T_{G} can be simply chosen by the following wavelength (λ) dependent transmittance:

$$T_{\mathrm{G}}(\lambda) = 1 + b\exp\left[-\frac{(\lambda-\lambda_0)^2}{(\Delta\lambda)^2}\right], \tag{11}$$

where $-1 \leqslant b < 0$ represents a narrowband Gaussian filter with an FWHM bandwidth of $2\sqrt{\ln 2}\Delta\lambda \simeq 1.665\Delta\lambda$; whereas $b > 0$ indicates a Gaussian-type amplifier. λ_0 is set as 2001.97 nm, deviated a little from that ($\approx$2001.75 nm) of the first sideband, which is so arranged to change less the spectrum of the eigensoliton. For a better illustration, we set $\Delta\lambda = 0.2$ nm, close to the bandwidth of the first sidebands ($\approx$0.3 nm), and choose $b = -1$ and 2 to implement a nearly 100% filtering and a triple spectral amplification, respectively. The filtering and the amplifying are performed behind the TDF. When a soliton is steadily circulating in the cavity, T_{G} in the two cases is then applied to the soliton only once at a fixed round trip. The spectral tailoring, though strong, only causes a weak disturbance to the soliton because only 3.2 and 6.3% of energy are lost and absorbed in the two cases, respectively. Application of the filter or the amplifier to the soliton is equivalent to a kind of transient interference without interaction, which directly leads to a small discontinuous frequency change.

It should be verified whether these jumped frequencies are retained in the recovery processes to respect the principle of momentum conservation. Figure 4(a) shows the narrowband Gaussian filter and amplifier at the two wavelengths of the first Gordon-Kelly sidebands, and Fig. 4(b) demonstrates the results in four spectral tailoring cases. After the spectral filtering, it can be seen that the frequency shifts due to the spectral losses mostly remain during two subsequent soliton recovery processes. However, the jumped frequencies slowly decline symmetrically for the redshift and the blueshift in the amplifier cases. This is because the excess amplification presents redundant DWs. In Fig. 4(b), the frequency shifts in the amplifier cases denoted by some balls are calculated via Eq. (8) by locating the peak of the eigensoliton or emergent soliton in each round trip to get $\delta(1/v_g)$, which just reflects the frequency shifting effect only for the eigensoliton. This implies the excess frequency jumps are from the stationary DW (soliton wings). It can be found that the eigen-

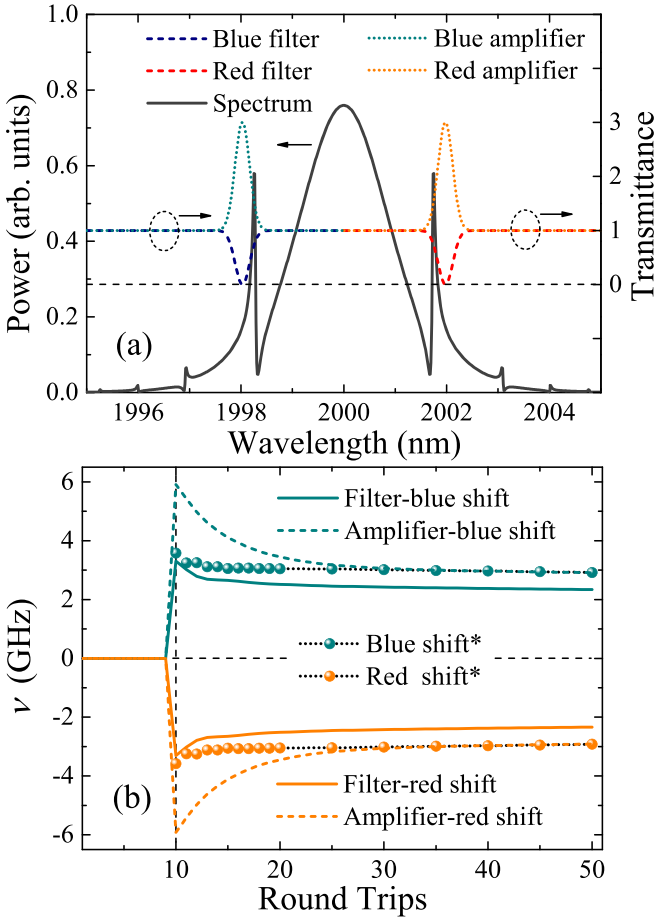

FIG. 4. (a) Transmittances of two Gaussian filters and two amplifiers with the original soliton spectrum and (b) the frequency shifts in the course of soliton recovery, started at the tenth round trip after a sudden spectral tailoring, where the scattered points are calculated by Eq. (8) in the amplifier cases (denoted by $*$).

soliton quickly reconstructs itself within five round trips and basically keeps its momentum after this "transient interference," whereas the soliton wings slowly transition and adjust over ten round trips. In the spectrum domain, when the soliton finishes its reconstruction, its new sideband pairs appear at new positions, which share the same mean momentum or frequency as those of the new soliton. In contrast, most parts of the old sidebands or overloaded DWs, abandoned by the new soliton, decay away and at the same time lose momentum apparently.

To see the details, the dynamic processes of the soliton are shown in Fig. 5. The negative chirp places the red and the blue sideband at the left and the right wing of the soliton, respectively, and the spectral tailoring works only on one side of the soliton pedestal, as seen from the figures. So, in the amplifier cases in Figs. 5(c) and 5(d), a large part of the enhanced sidebands is useless for the soliton; nevertheless, in the filter cases in Figs. 5(a) and 5(b), the residual soliton wings after cutting are much reduced and lead to a momentum loss. The above discussion reminds us to treat the eigensoliton and its accompanying DW separately. In spite of periodical pulsation, the eigensoliton is approximately nondissipative and close to the conventional soliton, so is almost conservative if not disturbed. The DWs as cavity resonant fields can survive long where the eigensoliton resides, the only place in which such a low loss can develop. Thus, they are highly dissipative and importantly nonconservative. As such, an effective interference that induces the frequency shift actually occurs between the incident DW and the eigensoliton. It explains the jump of momenta in Fig. 4(b) and the behaviors of the DWs in Figs. 5(c) and 5(d) under a sudden spectral tailoring.

Conclusively, a DW-soliton interaction will lead to frequency shifting of the soliton which is dominated by the interference and is mostly maintained in the soliton due to a subsequent momentum conservation process. In the time domain, we can find that the soliton adjusts itself by shedding an excess part of old DWs and by absorbing new frequencies from DWs or background like a breath, which is a reflection of its conservation and stability. Aside from the frequency shifting effect, the soliton oscillation is not found, but it is common in the extracavity case from an interference between the soliton and the DW [26,35]. This is possibly due to the shortness and dissipation of the incident DW.

C. DWMSI between two solitons

Actually, the DW-soliton interaction exists widely in multisoliton states, so the DWMSI can take effect for a low-loss case in which most DWs can survive over a sufficiently long time until they meet other solitons. To see a detailed nonstationary DWMSI process between solitons, we examine a simple case where soliton molecules (a bound soliton pair) are disturbed by each other to dissociate. A repulsive and an attractive DWMSI are simulated and demonstrated in Figs. 6(a) and 6(b), respectively. At first, a pair of bound solitons, separated by 250 ps, is triggered by two initial spikes and quickly becomes stable after 50 round trips with $E_{\mathrm{sat}} = 4.0$ pJ and $\theta = 0.7\pi$. At the round trip 60 then, θ is tuned to 0.6π to lower the mode-locking threshold, so as to raise soliton wings. It gives DWs a longer lifetime to arouse stronger interactions. For the attractive case in Fig. 6(b), the separation of two bound solitons is shifted to 251 ps, which reverses the phase difference between an emitted DW and a head-on soliton compared with that in Fig. 6(a). Obviously, the first pair of DWs generated by the angle switch plays an important role in the DW-soliton interaction since they have maximum energy due to the Q-switching-like effect. When a DW from one soliton first reaches the other one, a mechanical effect (repulsive or attractive) is then set off. Following the first pair of DWs, those subsequent DWs show a relatively weak strength and only disturb the solitons to fluctuate, which can be captured at a low-intensity scale. This phenomenon can be seen in Figs. 6(c) and 6(d), where, for a better view, the details are zoomed in from the rectangular areas in Figs. 6(a) and 6(b), respectively. Clearly, a consecutive perturbation by external DWs makes the two solitons interact indirectly by shedding DWs alternatively in two directions. So, it drives the solitons to wriggle [the soliton loci in Figs. 6(c) and 6(d) are marked by black lines], but does not affect their average motion, forming a kind of weak time jitter of solitons. During the DWMSI, the emitted DWs make up a complex nonstationary wave covering the two solitons. At round trip numbers over ≈ 240 in Fig. 6(a), it can be seen that the DWMSI ceases to work

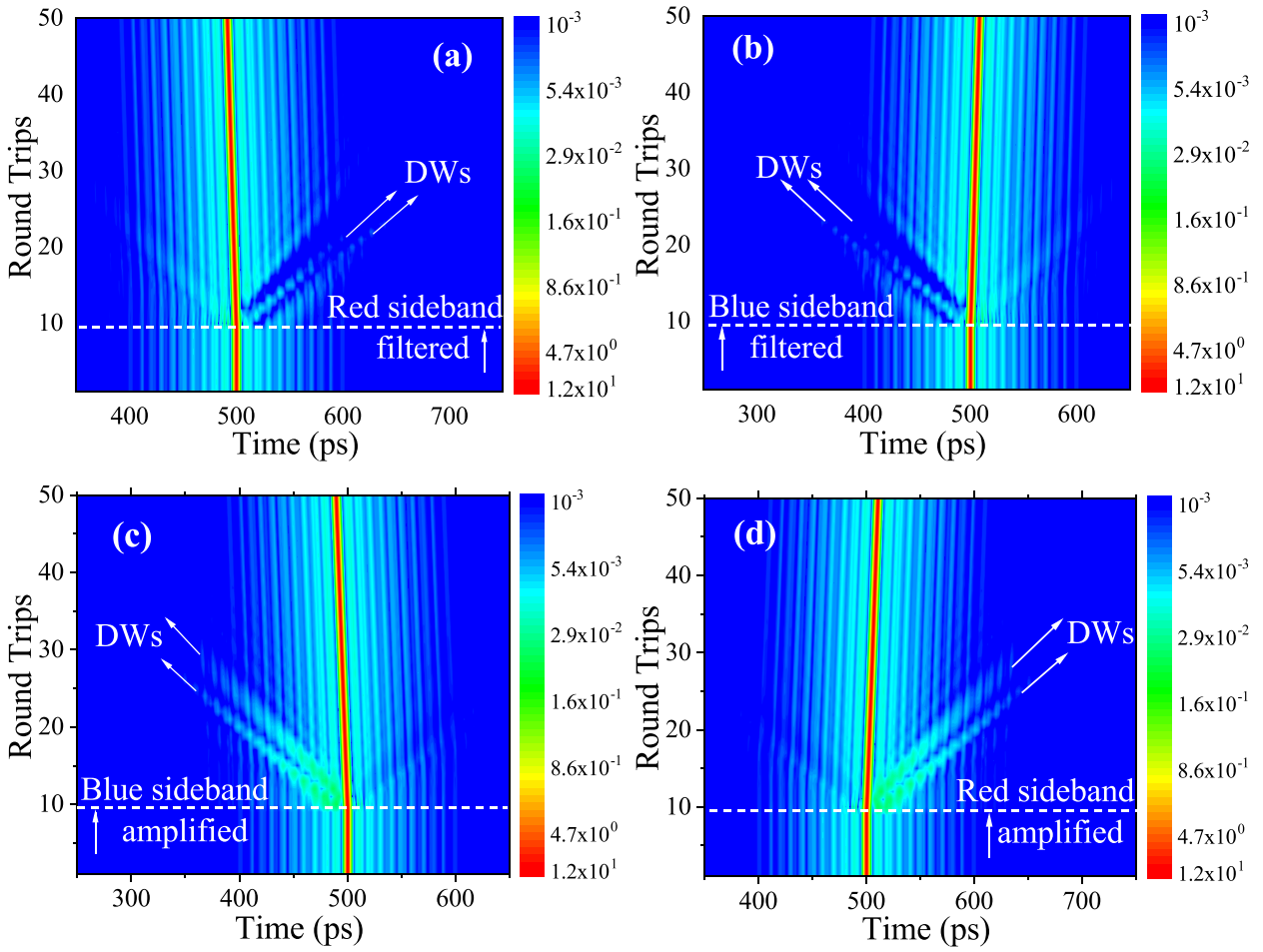

FIG. 5. Evolutions of the soliton in the cavity after filtering (a) the red and (b) the blue sideband, and after triply amplifying (c) the blue and (d) the red sideband, started at the tenth round trip.

and that the DW-soliton interaction still remains in the way of emitting overloaded DWs, self-interaction of solitons with their nonstationary DWs. In this case, the drifting solitons swing as another kind of time jitter, in a slow and a little random way due to an asymmetrical DW shedding. Such a motion can obviously not happen without an initial external perturbation (emitted DWs from another soliton). This swinging motion is different from those found in fiber lasers before, e.g., the soliton fluctuation in a fiber ring cavity mode locked by semiconductor saturable absorber mirror [65].

It is found that the conservation of momentum approximated by Eq. (10) is still able to explain the time-jittering motions. In this case, the conservation of momentum can yield weak spectral recoil when excess DWs shed from a soliton, i.e., the soliton is forced into a recoil movement once it emits DWs. A spectral recoil known to us is that a soliton gets a large group velocity shift by going across a zero dispersion point [45]. Owing to very small frequency differences of neighboring sidebands, the soliton here does not obtain an obvious jump of group velocity like the third-order dispersive soliton. Thus, the nonstationary DWs since appearing will constantly force its host, the soliton, to fluctuate, as is the case in Figs. 6(c) and 6(d). In the DWMSI regime at the round trips within 60–240 in Fig. 6(a) and 60–500 in Fig. 6(b), the interference and spectral recoil take effect together, resulting in a more frequent oscillation. Actually, the spectral recoil movement is similar to the frequency shifting process for the filter case in Figs. 5(a) and 5(b), if we take it as a momentum conserving motion of the emergent soliton after the sudden spectral tailoring. In such a way, the emergent soliton constantly relaxes into an eigensoliton by periodically emitting and absorbing DWs when suffering a periodical phase variation.

The above result indicates that a manipulation over solitons in a lumped cavity requires a suppression to the lifetime of DWs or a precise counteraction by an additional interaction, to artificially pattern multisoliton structures in practice [16,17].

IV. DISCUSSIONS ON INTERFERENCE

From the foregoing numerical results, already it is known that the interference induces the frequency shifting effect and explains the DW-soliton interaction and DWMSI as well. In spite of the nonlinear interaction, the interference works remarkably well in the mentioned dynamical phenomena. Generally, the interference happens when an interacting soliton radiates linear wave components, which will finally overlap with the incident DW. In this case, the DW packet

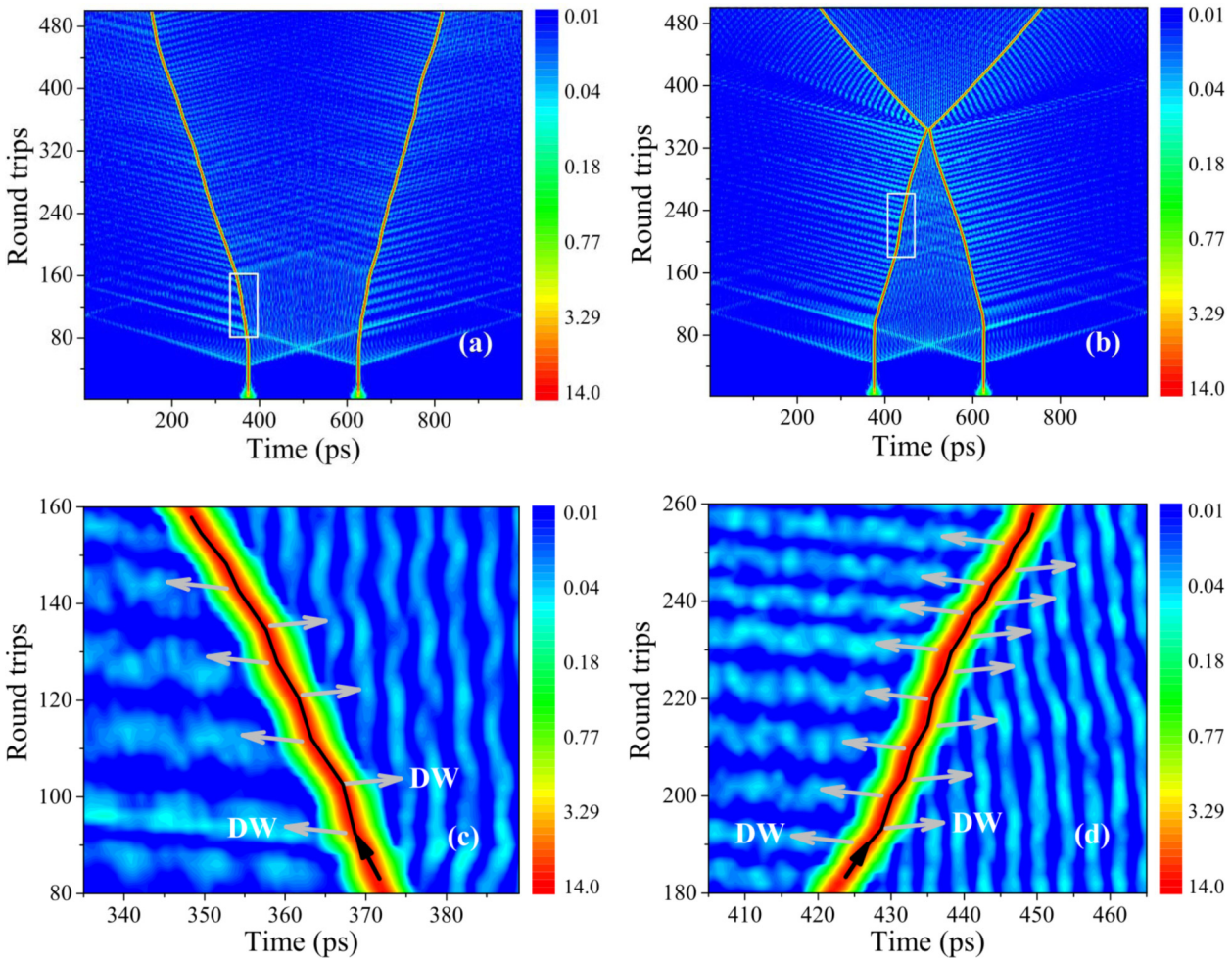

FIG. 6. Evolutions of two solitons during two DWMSIs in the cases of (a) a repulsive and (b) an attractive interaction initiated by the first DWs, with closeups of (c) the blueshifted and (d) the redshifted soliton zoomed in from the rectangle regions in upper subgraphs (a) and (b), respectively.

drains or releases energy from or to the soliton and turns into a new DW by interference with these wave components, as was studied by early researchers [22,23,25]. However, this phenomenon is only a consequence of the DW-soliton interaction, not a cause. Evidently, nonlinearities like SPM, XPM, and FWM are more essential in the interaction, even though they do not always show themselves. The interference mechanism in the context naturally has its nonlinear physical origin. The nonlinear effect in the soliton makes itself a dispersion-free pulse with a constant propagating mode, different from the frequency-dependent dispersion of a CW [22]. Owing to their mismatched mode constants over the bandwidth, the superimposed spectrum under interference varies periodically with distance [27], similar to a kind of spatial interference. It infers that the soliton and the CW are independent of each other according to classic (linear) optics, like two waves with different modes (so with different group velocities) propagating in a multimode fiber, which means they will completely restore when separating. In other words, the wave independence does not produce any interference effect between them finally. So, the interference primarily exists among the soliton and the nonlinear wave components induced by the SPM and XPM. Since the soliton state is the only low-energy eigen-non-linear wave, these induced nonlinear waves should have the same dispersion relation if they can survive in the abnormal dispersion cavity. Hence, the matching of their propagating mode constants, i.e., satisfying the phase-matching condition, is a self-evident premise for the interference between copropagating waves. Naturally during the DW-soliton interaction, the SPM- and XPM-induced nonlinear waves in the DW are mostly absorbed by the soliton through interference. In this case, importantly, the phase carried by the XPM-induced waves directly decides on the degree of interference (construction or destruction), then on the frequency shift of the soliton in the second scenario. According to the term "nonlinear interference" used by Kuznetsov *et al.* [35], the XPM-induced nonlinear interference mechanism may be more appropriate for the DW-soliton interaction in the first scenario, which will be revisited in the Appendices for more details.

Though the computations in this paper are limited to some simplifications, which preclude the birefringent dispersion, gain dynamics, FWM, and higher-order dispersion, to isolate the main characteristics of the interaction in an NPR mode-locked Tm-doped fiber ring laser, the results still have a meaning in broadly understanding the DW-soliton interaction and DWMSI.

V. CONCLUSIONS

In summary, the DW-soliton interaction and DWMSI are analyzed in detail by a simulation of the soliton generation in a weakly mode-locked fiber ring laser. It is found that an incident DW brings a distinct red or blue frequency shifting effect depending on the resonance at the Gordon-Kelly sidebands. The soliton without disturbance is observed to abide approximately by the conservation of momentum, as can be attributed to its stability. A quick soliton wiggling in DWMSI and a relatively slower fluctuation in a self-interaction are found at a low-loss mode-locking state. This kind of motion is caused by the spectral recoil movement in the background of nonstationary DWs, a consequence of the momentum conservation process of solitons. The DW-soliton interaction can be well explained by the nonlinear interference mechanism inside the first interacting scenario, which directly leads to a jump of the soliton momentum, and by the conservation of momentum in the second scenario of the recovery process. The XPM-induced nonlinear interference mechanism contributes to the understanding of soliton dynamics.

ACKNOWLEDGMENTS

This work was supported by National Natural Science Foundation of China (Grant No. 61775166), Natural Science Foundation of Tianjin (Grant No. 19JCZDJC32600), and Program for Innovative Research Team in University of Tianjin (Grant No. TD13-5035).

APPENDIX A: NONLINEAR INTERFERENCE

1. Interference mechanism in soliton perturbations

We will show further that a perturbation to single solitons, like that in the CW-soliton interaction, can be interpreted as an interference mechanism by a phenomenology method.

Let us consider a normalized scalar NSE for fundamental solitons [2], i.e.,

$$i\frac{\partial u}{\partial \xi}+\frac{1}{2}\frac{\partial^2 u}{\partial \bar{\tau}^2}+|u|^2u+f(u)=0, \tag{A1}$$

where the amplitude $u=A/\sqrt{P_0}=u(t;\bar{\tau},\xi)$ is scaled with the peak power P_0, normalized moving time $\bar{\tau}=\tau/\tau_0$, position $\xi=z|\beta_2|/\tau_0^2$, and $f(u)$ is a dissipative function related to a local gain and loss. In a two-wave collision case, we have $u=u_\mathrm{s}+u_\mathrm{c}$, indicating the superposition of a soliton u_s and a pulsed CW u_c, where the term CW, not DW, is used for a broader discussion. When their spectra overlap like that in a DW-soliton interaction, u_s and u_c are unambiguous and distinguishable only when they separate in the temporal domain. For a distinguishable two-wave case, we can adopt a widely used two-wave equation set satisfying

$$i\frac{\partial u_\mathrm{s}}{\partial \xi}+\frac{1}{2}\frac{\partial^2 u_\mathrm{s}}{\partial \bar{\tau}^2}+|u_\mathrm{s}|^2u_\mathrm{s}+f(u_\mathrm{s})=-2|u_\mathrm{c}|^2u_\mathrm{s}-u_\mathrm{c}^2u_\mathrm{s}^*, \tag{A2a}$$

$$i\frac{\partial u_\mathrm{c}}{\partial \xi}+\frac{1}{2}\frac{\partial^2 u_\mathrm{c}}{\partial \bar{\tau}^2}+|u_\mathrm{c}|^2u_\mathrm{c}+f(u_\mathrm{c})=-2|u_\mathrm{s}|^2u_\mathrm{c}-u_\mathrm{s}^2u_\mathrm{c}^*. \tag{A2b}$$

On the right-hand side of Eqs. (A2), the first term is from XPM and the last one is from FWM which generates new frequencies. The division of the FWM terms between u_s and u_c cannot be reasonably done in the two-wave case, so they are arbitrarily placed in the two subequations. Owing to a large phase mismatch ($L_\mathrm{B}\ll L$), the FWM contributes little to the interaction. In this case, u_c will undertake the main nonlinear effect at the beginning since $|u_\mathrm{c}|\ll|u_\mathrm{s}|$. Even though the CW-soliton interaction may be indistinguishable, Eqs. (A2) are effective as a starting point in a small signal case. In the quest for concision, we now use the brackets $\langle u_\mathrm{s},u_\mathrm{c}\rangle$ to denote their inner product as usual, i.e., $\int_{-\infty}^{\infty}u_\mathrm{s}^*u_\mathrm{c}d\bar{\tau}$. Then, the total energy of the superimposed wave is

$$E=\langle u_\mathrm{s},u_\mathrm{s}\rangle+\langle u_\mathrm{c},u_\mathrm{c}\rangle+\langle u_\mathrm{s},u_\mathrm{c}\rangle+\langle u_\mathrm{c},u_\mathrm{s}\rangle. \tag{A3}$$

The last two are interference terms. Thinking of $u_\mathrm{s}/\langle u_\mathrm{s},u_\mathrm{s}\rangle$ as a probability amplitude, we generalize Eq. (A3) to an arbitrary conservative physical quantity O, with its Hermite operator representation $\hat{O}$. Its mean value on the soliton state can be approximately expressed as

$$O\langle u_\mathrm{s},u_\mathrm{s}\rangle=\langle u_\mathrm{s},\hat{O}u_\mathrm{s}\rangle+\langle u_\mathrm{c},\hat{O}u_\mathrm{c}\rangle+\langle u_\mathrm{s},\hat{O}u_\mathrm{c}\rangle+\langle u_\mathrm{c},\hat{O}u_\mathrm{s}\rangle. \tag{A4}$$

Accordingly, the breath of the soliton by taking in a part of the CW and emitting residuals can be attributed to the last two terms in Eqs. (A3) and (A4), where the coupling matrix element can be called the generalized interference term, which is similar to that in quantum theory. In the CW-soliton interaction, the wave u can be rewritten as $u=u_\mathrm{ES}+u_\mathrm{c}'$ for an emergent soliton u_ES and a new CW u_c' with $\Delta u_\mathrm{c}=u_\mathrm{c}-u_\mathrm{c}'$. Now, phenomenologically, we assume that the emergent soliton absorbs Δu_c in the first scenario, which dominates the interference terms, so can no longer effectively interfere with the new CW u_c', i.e.,

$$\langle u_\mathrm{ES},\hat{O}u_\mathrm{c}'\rangle=0, \tag{A5}$$

which means their interference intensity $2\mathrm{Re}(u_\mathrm{ES}^*u_\mathrm{c}')$ will not cause any observable effect according to the phenomenological assumption. The emergent soliton u_ES has an implicit form in Eq. (A5) but is unnecessary to be known in the following development. Subsequently, in the second scenario, u_ES will relax to a stable eigensoliton u_s' possessing new parameters generated in u_ES out of subsequent conservations. Hence, Eq. (A4) can be rewritten as

$$\begin{aligned}O\langle u_\mathrm{ES},u_\mathrm{ES}\rangle&=\langle u_\mathrm{ES},\hat{O}u_\mathrm{ES}\rangle=\langle u,\hat{O}u\rangle-\langle u_\mathrm{c}',\hat{O}u_\mathrm{c}'\rangle\\&=\langle u_\mathrm{s},\hat{O}u_\mathrm{s}\rangle+2\mathrm{Re}[\langle u_\mathrm{s},\hat{O}u_\mathrm{c}\rangle]\\&\quad+\langle u_\mathrm{c},\hat{O}u_\mathrm{c}\rangle-\langle u_\mathrm{c}',\hat{O}u_\mathrm{c}'\rangle,\end{aligned} \tag{A6}$$

where the decoupling condition (A5) and the relation $\langle u_\mathrm{c},\hat{O}u_\mathrm{s}\rangle=\langle u_\mathrm{s},\hat{O}u_\mathrm{c}\rangle^*$ are applied. The quantity O in Eq. (A6) is purposely expanded according to u_s and u_c because they are obtainable from Eqs. (A2) upon a short-range interaction. In the conservative scenario, it indicates an asymptotic process

$$u_\mathrm{ES}\xrightarrow{\xi\to\infty}u_\mathrm{s}',\ \langle u_\mathrm{ES},\hat{O}u_\mathrm{ES}\rangle\xrightarrow{\xi\to\infty}\langle u_\mathrm{s}',\hat{O}u_\mathrm{s}'\rangle \tag{A7}$$

from Eq. (A6). Then, u_s' will result from O. The main terms in Eq. (A6) include a basic quantity O_0 and the first-order

variation δO, i.e.,

$$O_0 = \frac{\langle u_s, \hat{O}u_s\rangle}{\langle u_s', u_s'\rangle}, \delta O = \frac{2\mathrm{Re}[\langle u_s, \hat{O}u_c\rangle]}{\langle u_s', u_s'\rangle}, \tag{A8}$$

which, before applying to other physical quantities, should be first used to estimate the energy $E = \langle u_s', u_s'\rangle$ of the new soliton. The last two terms in Eq. (A6) are commonly neglected to the first order of the CW. Consequently, δO from u_c becomes the main perturbation, which just is the interference term. Since an exact u_{ES} is hard to find, Eq. (A5) can be substituted by $\langle u_s, \hat{O}u_c'\rangle = 0$ to search for an approximate solution to u_c'. Just with the method developed by Gordon *et al*, some approximate solutions can be found in a few perturbation cases [22,25]. For a given u_c', a more exact O can be resulted from Eq. (A6). Equations (A8) can be verified by some known perturbative results of conventional solitons. The fundamental soliton solution of Eq. (A1) with $f = 0$ can be expressed by [2]

$$u_s = \eta\mathrm{sech}[\eta(\bar{\tau} - \bar{\tau}_s - \omega\xi)]\exp[i(\phi_s - \omega\bar{\tau})], \tag{A9}$$

where η, $\omega = \Omega\tau_0$, $\bar{\tau}_s$, and ϕ_s represent the amplitude around the unit, scaled circular frequency, soliton position, and phase factor, respectively. The four parameters, mostly used to characterize a soliton, are conservative without an outside disturbance. In this case, we have $\langle u_s, u_s\rangle = 2\eta$, thus the perturbation in Eq. (A8) turns into

$$\eta\delta O = \mathrm{Re}[\langle u_s, \hat{O}u_c\rangle]. \tag{A10}$$

By choosing the operators of the amplitude η, frequency $i\partial/\partial\bar{\tau}$, time $\bar{\tau}$, and chirp $i\bar{\tau}\partial/\partial\bar{\tau}$, we have the following perturbations:

$$\delta\eta = \mathrm{Re}[\langle u_s, u_c\rangle], \tag{A11a}$$

$$\eta\delta\omega = -\mathrm{Im}[\langle u_s, \partial u_c/\partial\bar{\tau}\rangle], \tag{A11b}$$

$$\eta\delta\bar{\tau}_s = \mathrm{Re}[\langle u_s, \bar{\tau}u_c\rangle], \tag{A11c}$$

$$\eta(\delta\phi_s + \omega\delta\bar{\tau}_s) = -\mathrm{Im}[\langle u_s, \bar{\tau}\partial u_c/\partial\bar{\tau}\rangle], \tag{A11d}$$

expressed as some generalized interference terms. In Eq. (A11 d), the chirp is an expectation of the product of instant frequency and time, which not only comes from a variation of the phase ϕ_s along time but also from a shift of the soliton position $\bar{\tau}_s$. Equations (A11) reproduce the standard results from the perturbation theories [22,66–68]. The derivation above is a refined version of the work of Gordon and Haus in Ref. [66], where, equivalently, Eq. (A4) was approximated by directly removing the second term on the right-hand side. The perturbation theory has been successfully applied in some simplified lumped cases [22,26].

From the numerical results in the paper and the perturbation analysis above, the interference mechanism plays an important role in the DW-soliton interaction. But, it is not yet a conventional interference because the CW carries a nonlinear effect, which will be shown next.

2. Nonlinearity in the interference mechanism

How nonlinearity plays a role needs to be known as to how it gets involved in energy exchange, and furthermore how it activates the interference.

For simplicity, we consider a distributed model with the balance of gain and loss upon a steady lasing operation, where an average of f over the cavity is then zero. In this case, a growth of u_c, neglecting a small SPM term, can be obtained as $\Delta u_c + \delta u_c$ by Eq. (A2 b) along a short distance $\delta\xi$, where

$$\Delta u_c \simeq i\big(2|u_s|^2u_c + u_s^2u_c^*\big)\delta\xi, \tag{A12}$$

and δu_c is the component of a pure dispersive variation in $\partial^2u_c/\partial\bar{\tau}^2$, but will not cause a nonzero perturbation according to Gordon's analysis [22]. It is an initial cross-phase-modulated wave imposed by the soliton, and also is a nonlinear wave carrying nearly the same frequency as that of the incident CW if neglecting the second term in Eq. (A12). The existence of the interference of this phase-modulated wave with the soliton becomes a natural conjecture. However, the abnormal dispersion stretches the initial phase-modulated wave which counteracts the SPM- and XPM-induced compression, such as that in a soliton. Thus the propagation property of these phase-modulated waves needs to be uncovered. Therefore, we simulate a hypothetical DW-soliton interaction via polarized Eqs. (A2), i.e., Eqs. (B3) (see Appendix B). This kind of simulation, for a demonstration of the phase-modulated waves, keeps the nonlinearity but excludes the interference between the soliton and DW involved. The initialization is chosen nearly the same as that in Fig. 3(b), but with a nonoptimal phase difference. The simulation results are shown in Fig. 7. It is a sure sign that neither u_s nor u_c in Fig. 7 represents a real soliton or DW, and that only their superposition or interference $u = u_s + u_c$ in Fig. 7(c) is correct. In such a simulation, the cross-phase-modulated wave induced by the soliton is automatically separated from that induced by the DW through Eqs. (A2), so can be numerically diagnosed during the interaction. The purpose of this separation is to help us to observe the dispersion and the interference way of the nonlinear waves.

At the beginning, the CW in the overlapping region becomes a phase-modulated wave as Eq. (A12). But with the growth of u_c, its impacts of XPM on the soliton and SPM on itself are strong enough to change the soliton. It is found in Figs. 7(a) and 7(b) that u_s and u_c each develop into a pair of solitary pulses with nearly the same amplitude, denoted by "1" for the redshifting subpulse and "2" for the blue one. This bifurcation is common in our simulation since u_c always grows into a solitary wave even when the intensity of the incident DW is ten times lower, no matter what value their phase difference takes. The interaction process completes in a period of ten round trips, which is demonstrated in Fig. 7(d), where, we can see the quickly accumulated phase-modulated waves (SPM+XPM) from both the initial soliton and the DW within the round trips from 12 to 20. The total field u in Fig. 7(c), however, is a blueshifting soliton as before, which means the parts of "1" in Figs. 7(a) and 7(b) cancel each other, nevertheless, the subpulses of "2" are superimposed to become a real soliton. This means that the phase-modulated waves and the soliton can be effectively interfered with since they have the same soliton dispersion relation (mode constant). It is a phase-matching condition, requiring two propagating mode constants to be equal to each other, which can be verified by the dispersion-free property in Fig. 7. Thus, different from an ordinary two-wave interaction, all the phase-modulated waves

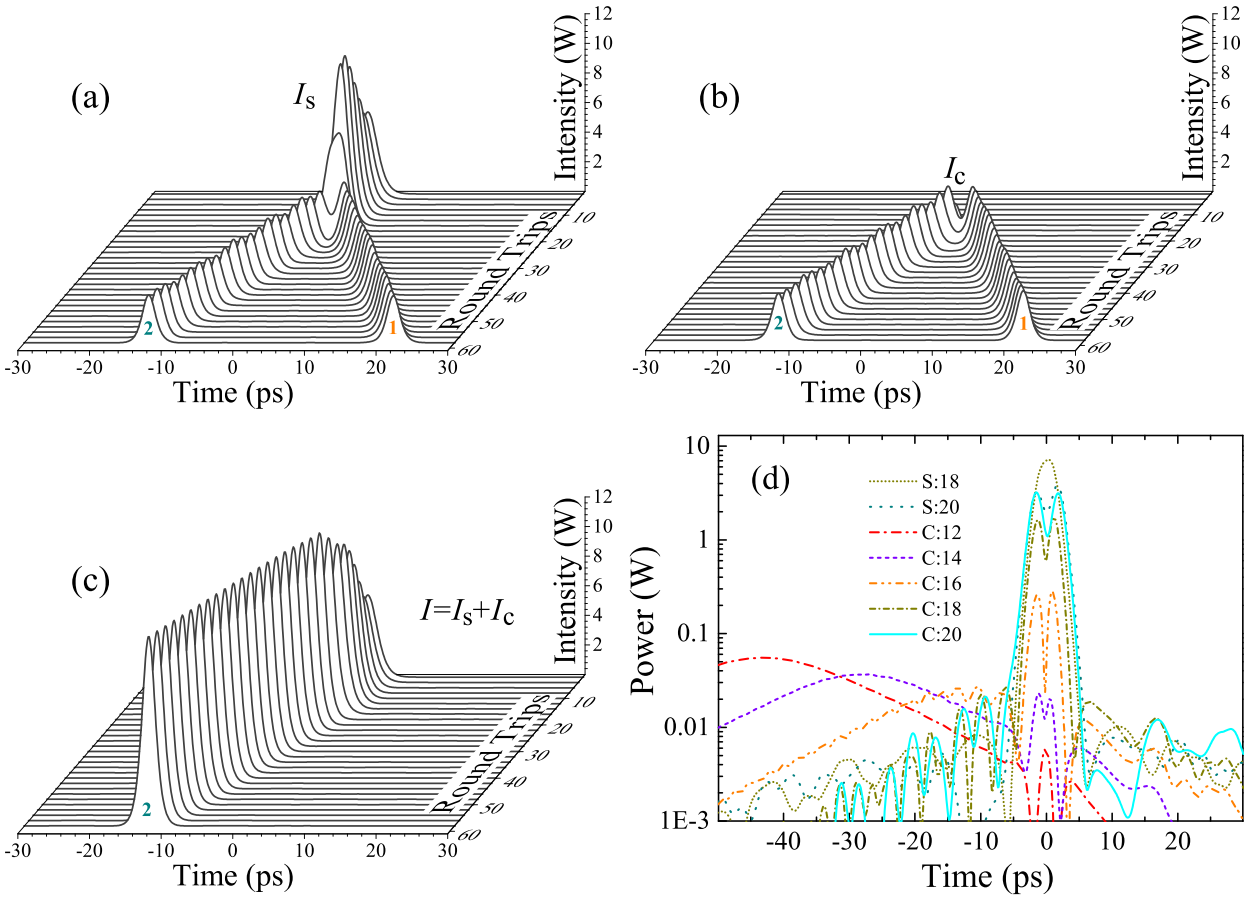

FIG. 7. Noninterference evolutions of (a) an initial soliton, (b) an incident DW, (c) real soliton evolution from their superposition, and (d) sampled interaction details, respectively, in a simulated DW-soliton interaction within 60 round trips by Eqs. (B3), where the related pulse intensities are indicated by I, I_s, and I_c with the notations "s" for soliton and "c" for CW and DW followed by round trip numbers.

couple back into the soliton step by step, which gives rise to an unbalanced XPM with phase-dependent momentum transfer. During this DW-soliton interaction in the first scenario, the interference of the soliton with the XPM-induced (by soliton) nonlinear wave plays a primary role since it carries the phase difference of the soliton and DW that determines a subsequent frequency shifting effect.

The result supports the aforementioned phenomenological assumption as well. Since Eqs. (A2) are unable to fully describe the CW and the soliton (output of unreal CW and soliton), it will be more meaningful for us to regard the total wave u phenomenologically as $u_{ES} + u_c'$. For the strong nonlinear effect, Eqs. (A11) are generally invalid, but still hold for such a case in which each interaction step over a small $\delta\xi$ can be decomposed into two scenarios as before. As such, the phase-modulated wave Δu_c merges from u_c into u_{ES} in the first scenario by interference while the SPM in u_{ES} takes over the next, where the two processes actually take place simultaneously in practice. u_c then becomes u_c' to go into the next step as a new incident DW, which will make Eqs. (A11) applicable in practice in spite of unavoidable complexity. It is then confirmed that the interference here can be taken as an XPM-induced nonlinear interference according to the discussions.

APPENDIX B: TWO-WAVE CGLEs

In terms of Eqs. (1), Eqs. (A2) can be forged into a vector version of CGLE in consideration of polarization states. This can be done through the substitutions $u\sqrt{P_0} \to A_{1,2}$, $u_s\sqrt{P_0} \to A_{s1,2}$, and $u_c\sqrt{P_0} \to A_{c1,2}$. Since the amplitudes $A_{s1/2}$ will couple with $A_{c1,2}$, the pairs $(A_{s1,2}, A_{c1,2})$ can be used in the new polarized two-wave equations. In addition, a further transformation of amplitudes should be used to make the traditional split-step method effective, i.e.,

$$U_{+1,2} = (A_{s1,2} + A_{c1,2})/\sqrt{2}, \tag{B1a}$$

$$U_{-1,2} = (A_{s1,2} - A_{c1,2})/\sqrt{2}, \tag{B1b}$$

where the real amplitudes A_s and A_c can be easily resolved through a matrix inversion on Eqs. (B1), and have the same expressions as above:

$$A_{s1,2} = (U_{+1,2} + U_{-1,2})/\sqrt{2}, \tag{B2a}$$

$$A_{c1,2} = (U_{+1,2} - U_{-1,2})/\sqrt{2}. \tag{B2b}$$

In this case, U_+ and U_- decouple in the nonlinear terms of a new CGLE, which can be derived from Eqs. (1) as

$$\frac{\partial U_{\pm1}}{\partial z} = \frac{g-\alpha}{2}U_{\pm1} + 2i\gamma\left(|U_{\pm1}|^2 + \tfrac{2}{3}|U_{\pm2}|^2\right)U_{\pm1} + \left(\frac{g}{2\Omega_g^2} - i\frac{\beta_2}{2}\right)\frac{\partial^2 U_{\pm1}}{\partial\tau^2} - \sigma\frac{\partial U_{\pm1}}{\partial\tau}, \tag{B3a}$$

$$\frac{\partial U_{\pm2}}{\partial z} = \frac{g-\alpha}{2}U_{\pm2} + 2i\gamma\left(|U_{\pm2}|^2 + \tfrac{2}{3}|U_{\pm1}|^2\right)U_{\pm2} + \left(\frac{g}{2\Omega_g^2} - i\frac{\beta_2}{2}\right)\frac{\partial^2 U_{\pm2}}{\partial\tau^2} + \sigma\frac{\partial U_{\pm2}}{\partial\tau}. \tag{B3b}$$

It should be noted that the nonlinear coefficient in Eqs. (B3) is doubled as $2i\gamma$.

[1] T. Dauxois and M. Peyrard, *Physics of Solitons* (Cambridge University, Cambridge, England, 2015).
[2] G. P. Agrawal, *Nonlinear Fiber Optics* (Academic, New York, 2001); *Applications of Nonlinear Fiber Optics* (Academic, New York, 2008).
[3] S. Chouli and P. Grelu, Phys. Rev. A **81**, 063829 (2010).
[4] F. Amrani, A. Haboucha, M. Salhi, H. Leblond, A. Komarov, and F. Sanchez, Appl. Phys. B **99**, 107 (2010).
[5] P. Grelu and N. Akhmediev, Nat. Photonics **6**, 84 (2012).
[6] Z. Q. Wang, K. Nithyanandan, A. Coillet, P. Tchofo-Dinda, and P. Grelu, Nat. Commun. **10**, 830 (2019).
[7] P. Grelu, *Nonlinear Optical Cavity Dynamics* (Wiley, New York, 2016)
[8] X. Liu, D. Popa, and N. Akhmediev, Phys. Rev. Lett. **123**, 093901 (2019).
[9] X. Liu and M. Pang, Laser Photonics Rev. **13**, 1800333 (2019).
[10] A. Mahjoubfar, D. V. Churkin, S. Barland, N. Broderick, S. K. Turitsyn, and B. Jalali, Nat. Photonics **11**, 341 (2017).
[11] G. Herink, F. Kurtz, B. Jalali, D. R. Solli, and C. Ropers, Science **356**, 50 (2017).
[12] P. Ryczkowski, M. Närhi, C. Billet, J.-M. Merolla, G. Genty, and J. M. Dudley, Nat. Photonics **12**, 221 (2018).
[13] Y. Wang, F. Leo, J. Fatome, M. Erkintalo, S. G. Murdoch, and S. Coen, Optica **4**, 855 (2017).
[14] Y. Zhou, Y. Ren, J. Shi, H. Mao, and K. K. Y. Wong, Optica **7**, 965 (2020).
[15] N. Englebert, C. M. Arabí, P. Parra-Rivas, S.-P. Gorza, and F. Leo, Nat. Photonics **15**, 536 (2021).
[16] M. Pang, W. He, X. Jiang, and P. St. J. Russell, Nat. Photonics **10**, 454 (2016).
[17] W. He, M. Pang, D. H. Yeh, J. Huang, C. R. Menyuk, and P. St. J. Russell, Nat. Commun. **10**, 5756 (2019).
[18] W. He, M. Pang, D.-H. Yeh, J. Huang, and P. St. J. Russell, Light: Science & Applications **10**, 120 (2021).
[19] K. Smith and L. F. Mollenauer, Opt. Lett. **14**, 1284 (1989).
[20] W. H. Loh, A. B. Grudinin, V. V. Afanasjev, and D. N. Payne, Opt. Lett. **19**, 698 (1994).
[21] D. Y. Tang, B. Zhao, L. M. Zhao, and H. Y. Tam, Phys. Rev. E **72**, 016616 (2005).
[22] J. P. Gordon, J. Opt. Soc. Am. B **9**, 91 (1992).
[23] M. W. Chbat, P. R. Prucnal, M. N. Islam, C. E. Soccolich, and J. P. Gordon, J. Opt. Soc. Am. B **10**, 1386 (1993).
[24] A. B. Grudinin and S. Gray, J. Opt. Soc. Am. B **14**, 144 (1997).
[25] H. A. Haus, W. S. Wong, and F. I. Khatri, J. Opt. Soc. Am. B **14**, 304 (1997).
[26] L. Socci and M. Romagnoli, J. Opt. Soc. Am. B **16**, 12 (1999).
[27] R. Weill, A. Bekker, V. Smulakovsky, B. Fischer, and O. Gat, Phys. Rev. A **83**, 043831 (2011).
[28] A. Komarov, F. Amrani, A. Dmitriev, K. Komarov, D. Meshcheriakov, and F. Sanchez, Phys. Rev. A **85**, 013802 (2012).
[29] E. M. Dianov, A. V. Luchnikov, A. N. Pilipetskii, and A. N. Starodumov, Opt. Lett. **15**, 314 (1990).
[30] A. N. Pilipetskii, E. A. Golovchenko, and C. R. Menyuk, Opt. Lett. **20**, 907 (1995).
[31] J. K. Jang, M. Erkintalo, S. G. Murdoch, and S. Coen, Nat. Photonics **7**, 657 (2013).
[32] Z. Wang, Z. Wang, Y. Liu, R. He, J. Zhao, G. Wang, and G. Yang, Opt. Lett. **43**, 478 (2018).
[33] R. Weill, A. Bekker, V. Smulakovsky, B. Fischer, and O. Gat, Optica **3**, 189 (2016).
[34] K. Sulimany, O. Lib, G. Masri, A. Klein, M. Fridman, P. Grelu, O. Gat, and H. Steinberg, Phys. Rev. Lett. **121**, 133902 (2018).
[35] E. A. Kuznetsov, A. V. Mikhailov, and I. A. Shimokhin, Physica D **87**, 201 (1995).
[36] H. A. Haus, F. I. Khatri, W. S. Wong, E. P. Ippen, and K. R. Tamura, IEEE J. Quantum Electron. **32**, 917 (1996).
[37] Q.-H. Park and H. J. Shin, Phys. Rev. Lett. **82**, 4432 (1999).
[38] H. J. Shin, Phys. Rev. E **63**, 026606 (2001); **67**, 017602 (2003).
[39] N. N. Akhmediev and S. Wabnitz, J. Opt. Soc. Am. B **9**, 236 (1992).
[40] B. Zhao, D. Y. Tang, P. Shum, W. S. Man, H. Y. Tam, Y. D. Gong, and C. Lu, Opt. Commun. **229**, 363 (2004).
[41] A. Komarov, K. Komarov, H. Leblond, and F. Sanchez, J. Opt. A **9**, 1149 (2007).
[42] F. Sanchez, P. Grelu, H. Leblond, A. Komarov, K. Komarov, M. Salhi, A. Niang, F. Amrani, C. Lecaplain, and S. Chouli, Opt. Fiber Technol. **20**, 562 (2014).
[43] A. Demircan, S. Amiranashvili, and G. Steinmeyer, Phys. Rev. Lett. **106**, 163901 (2011).
[44] A. V. Yulin, R. Driben, B. A. Malomed, and D. V. Skryabin, Opt. Express **21**, 14481 (2013).
[45] N. Akhmediev and M. Karlsson, Phys. Rev. A **51**, 2602 (1995).
[46] C. Milián and D. V. Skryabin, Opt. Express **22**, 3732 (2014).
[47] A. Efimov, A. V. Yulin, D. V. Skryabin, J. C. Knight, N. Joly, F. G. Omenetto, A. J. Taylor, and P. Russell, Phys. Rev. Lett. **95**, 213902 (2005).
[48] D. V. Skryabin and A. V. Gorbach, Rev. Mod. Phys. **82**, 1287 (2010).
[49] S. M. J. Kelly, Electron. Lett. **28**, 806 (1992).
[50] N. J. Smith, K. J. Blow, and I. Andonovic, J. Lightwave Technol. **10**, 1329 (1992).
[51] J. M. Soto-Crespo, N. Akhmediev, P. Grelu, and F. Belhache, Opt. Lett. **28**, 1757 (2003).

[52] P. Wang, X. Xiao, and C. Yang, Opt. Lett. **42**, 29 (2017).
[53] A. Komarov, K. Komarov, A. Niang, and F. Sanchez, Phys. Rev. A **89**, 013833 (2014).
[54] A. Niang, F. Amrani, M. Salhi, H. Leblond, A. Komarov, and F. Sanchez, Opt. Commun. **312**, 1 (2014).
[55] G. Semaan, A. Komarov, M. Salhi, and F. Sanchez, Opt. Commun. **387**, 65 (2017).
[56] D. Y. Tang, S. Fleming, W. S. Man, H. Y. Tam, and M. S. Demokan, J. Opt. Soc. Am. B **18**, 1443 (2001).
[57] C.-J. Chen, P. K. A. Wai, and C. R. Menyuk, Opt. Lett. **17**, 417 (1992).
[58] Y. Li, C. Lou, J. Wu, B. Wu, and Y. Gao, IEEE Photon. Technol. Lett. **10**, 1250 (1998).
[59] H. E. Kotb, M. A. Abdelalim, and H. Anis, IEEE J. Select. Topics Quantum Electron. **20**, 1100809 (2014).
[60] X. Liu, Phys. Rev. A **84**, 053828 (2011).
[61] E. Ding and J. N. Kutz, J. Opt. Soc. Am. B **26**, 2290 (2009).
[62] A. Zaviyalov, R. Iliew, O. Egorov, and F. Lederer, J. Opt. Soc. Am. B **27**, 2313 (2010).
[63] *Dissipative Solitons: From Optics to Biology and Medicine*, edited by N. Akhmediev and A. Ankiewicz, Lecture Notes in Physics Vol. 751 (Springer, Berlin, Heidelberg, 2008).
[64] Y. Du, X. Shu, H. Cao, and P. Cheng, IEEE J. Select. Topics Quantum Electron. **24**, 1101408 (2018).
[65] D. A. Korobko, R. Gumenyuk, I. O. Zolotovskii, and O. G. Okhotnikov, Optical Fiber Technology **20**, 593 (2014).
[66] J. P. Gordon and H. A. Haus, Opt. Lett. **11**, 665 (1986).
[67] H. A. Haus and Y. Lai, J. Opt. Soc. Am. B **7**, 386 (1990).
[68] H. A. Haus and W. S. Wong, Rev. Mod. Phys. **68**, 423 (1996).